Int. J. Electrochem. Sci., 9 **(2014)** 1583 - 1596

International Journal of ELECTROCHEMICAL SCIENCE
www.electrochemsci.org

Structure and Electrochemical Properties of Spinel $Li_4Ti_5O_{12}$ Nanocomposites as Anode for Lithium-Ion Battery

Xiangcheng Sun[1,], Manu Hegde[2], Yuefei Zhang[3], Min He[4], Lin Gu[4], Yongqing Wang[5], Jie Shu[6], Pavle V. Radovanovic[2], and Bo Cui[1]*

[1]Department of Electrical and Computer Engineering, University of Waterloo, Canada
[2]Department of Chemistry, University of Waterloo, Canada
[3]Institute of Microstructure and Property of Advanced Materials, Beijing University of Technology, Beijing 100022, PR China
[4]Beijing National Laboratory for Condensed Matter Physics, Institute of Physics, Chinese Academy of Sciences, Beijing 100190, PR China
[5]Institute of Chemistry, Chinese Academy of Sciences, Beijing 100190, PR China
[6]Faculty of Materials Science and Chemical Engineering, Ningbo University, 315211, PR China
[*]E-mail: sunxc824@gmail.com

Received: 1 November 2013 / *Accepted:* 31 December 2013 / *Published:* 2 February 2014

Nanocomposite particles of amorphous carbon-$Li_4Ti_5O_{12}$ (C-LTO) and carbon nanotube-$Li_4Ti_5O_{12}$ (CNT-LTO) were synthesized by solvothermal method and subsequent high-temperature calcination. X-ray diffraction (XRD), transmission electron microscopy (TEM), high-resolution transmission electron microscopy (HR-TEM), and selected area electron diffraction (SAED) were applied to characterize the phase structure, particle morphology, and the coating structure. XRD analysis, TEM micrographs, HR-TEM images and SAED analysis revealed that both LTO particles exhibited a well-developed spinel nanocrystal structure with average sizes between 20-70 nm. The C-LTO particles exhibited roughly spherical shape coated by an amorphous carbon layer up to 10 nm in thickness. The CNT-LTO samples showed uniform square nanocrystals with edge length around 20 nm and nanoscale graphitic layers covering the surface, revealing the carbon nanotubes interconnection networks among the particle assemblies. Electrochemical studies of lithium insertion/extraction performance are evaluated by the galvanostatic charge/discharge tests, cyclic voltammetry (CV) and electrochemical impedance spectroscopy (EIS). Both LTO particles showed the superior initial discharge capacity of more than 200 mAh/g at 1/10C rate. The irreversible capacity of the C-LTO particles at more cycles was due to large polarization resulted from excessive carbon and possible residual precursors. The CNT-LTO particles show larger reversible capacity and enhanced electrochemical Li^+ insertion/extraction kinetics at different cycling rates. The comparative structural and electrochemical analyses demonstrated that both nanoscale graphitic covering layers and the CNT interconnection networks increase the electronic conductivity and improve the kinetics rates of lithium insertion/extraction in the CNT-LTO particles.

Keywords: Lithium-ion battery, $Li_4Ti_5O_{12}$, X-ray diffraction, electron microscopy, amorphous coating, lithium insertion/extraction

1. INTRODUCTION

As an alternative anode material for lithium ion batteries (LIBs), spinel lithium titanate ($Li_4Ti_5O_{12}$, LTO) offers higher safety and longer cycle life (due to the negligible volume change) than the currently commercial carbon (graphite) anode materials [1-14]. The spinel-type LTO showed excellent structural stability of almost zero-strain during lithium ion insertion/extraction, leading to high rate capability and reversibility during discharge-charge cycling. It also provides a stable voltage of 1.55 V against a lithium electrode with a theoretical capacity of 175 mAh/g and an actual discharge capacity of over 160 mAh/g [2, 3]. Furthermore, $Li_4Ti_5O_{12}$ is cheap and non-toxic, and is easier to produce than other alloy-based anodes [1-9]. As it does not act as a Li^+ ion source during charge-discharge process, $Li_4Ti_5O_{12}$ needs to be coupled with a 4 V cathode such as $LiFePO_4$ to provide a battery cell with an operating voltage of approximately 2.5 V. It has been reported that lithium reacts with $Li_4Ti_5O_{12}$ according to the kinetic reaction $Li_4Ti_5O_{12} + 3Li^+ + 3e \rightarrow Li_7Ti_5O_{12}$, where lithium insertion into the $Li_4Ti_5O_{12}$ spinal displaces tetrahedrally coordinated lithium ions into octahedral sites, resulting in the formation of a rock salt-type $Li_7Ti_5O_{12}$ crystals [1, 3]. The rate capability of $Li_4Ti_5O_{12}$ is relatively low, as the poor electrical conductivity and slow lithium-ion diffusion lead to large polarization at high charge–discharge rates [5-8].

So far, various doping, mixing and coating techniques were used to improve the electronic conductivity and electrochemical properties of $Li_4Ti_5O_{12}$ [10-13]. The most effective way to improve their rate performance is the well-known surface carbon-coating technique, which improves the surface electronic conductivity and the electric contact between particles and conducting agents, leading to a significantly improved electrochemical performance. However, most of the previous efforts have been focused on controlling the crystallinity, thickness and uniformity of the carbon coating layer [8-17]. Another effective approach is to produce nano-architectures of $Li_4Ti_5O_{12}$ materials such as nanowires and nanorods that can facilitate both electron and lithium ion transport by reducing the diffusion paths [16-20]. Much research effort has been paid to carbon-coated $Li_4Ti_5O_{12}$ nano-materials that have demonstrated improvement in the cycling and rate performance [20-29]. However, the question of how the carbon (i.e. how much content) and active materials connect to each other and what the interfacial structure between them still needs to be clarified.

In this paper, we carried out the comparative experimental characterization and electrochemical testing of C-$Li_4Ti_5O_{12}$ and CNT-$Li_4Ti_5O_{12}$ composite particles. Our result showed that the nanoscale graphitic covering layers and the CNT interconnection networks between CNT-LTO isolated particles, gives rise to the effective interconnects that results in enhanced electronic conductivity and electrochemical properties.

2. EXPERIMENTAL METHODS

2.1 Solvothermal synthesis and solid-state reaction

First of all, micro-size Li-Ti-O precursors were solvothermally synthesized using commercial anatase TiO_2 powders (e.g., 25 nm) as raw precursors. In a typical synthesis, a stoichiometric amount (i.e., Ti:Li=5:4) of anatase TiO_2 powder (0.4 g) was dispersed in $LiOH \cdot H_2O$ aqueous solution (60 ml). After stirring for 30 min, the suspension was transferred into a 50 mL Teflon-lined autoclave and heated at 180^{o}C for 24 hrs. Subsequently, the white precipitate was separated by filtration, and washed several times with deionized water to remove the excess hydroxides before drying at 80^{o}C for 6 hr. Finally, the micro-size Li-Ti-O white powder was mixed with multi-wall carbon nanotube and conducting black carbon powder, and the two different powder mixtures were calcinated respectively at 800^{o}C and 900^{o}C for 5 hr under Ar gas, followed by gradual cooling in the furnace.

2.2 Structure Characterizations

The morphologies of as-prepared C-LTO and CNT-LTO nanocomposite particles were characterized by scanning electron microscopy and transmission electron microscopy (TEM). Crystal nanostructures were analyzed by powder X-ray diffraction (XRD) with a INEL XRG 3000 diffractometer operating in transmission mode with Cu Ka radiation (λ= 0.15418 nm). Phase identification and carbon coating structure of both C-LTO and CNT-LTO particles were characterized and examined by high resolution TEM imaging (HR-TEM) and selected-area electron diffraction (SAED) using a JEOL 2010F FEG TEM at an accelerating voltage of 200 kV. In addition to TEM, the carbon coating contents were quantitated by scanning electron microscopy (ZEISS Ultra Plus equipped with EDX detector).

2.3 Battery preparation and electrochemical testing

Both C-LTO and CNT-LTO nanocomposite materials were examined using a CR2016 coin-type cell for which the lithium metal was used as a counter electrode. To fabricate the anodes for the battery test cells, the working electrode was prepared as follows. Active materials (87%) were mixed with acetylene black (8%) as conducting agent, and polyvinylidene fluoride (PVDF)(5%) as binder in N-methylpyrrolidine (NMP). The blended slurries were pasted onto a copper current collector, and the electrode was dried at 80^{o}C for 12 h in a vacuum oven. The electrolyte used was 1M LiPF6 solvent in a 1:1:1 (vol%) mixture of ethylene carbonate (EC), ethylmethyl carbonate (EMC), and dimethyl carbonate (DMC). Test cells were assembled in an argon-filled glove box using Li foil as the counter electrode and polypropylene (PP) film as the separator. Galvanostatic charge-discharge cycling tests for both coin cells were performed within a range of 1.0 V-3.0 V versus the Lithium counter electrode using a CT2001A cell test instrument (LAND Electronic Co). The specific capacities of the samples were calculated based on the mass of the composites. The cyclic voltammetry (CV) for both coin cells was performed using the Arbin 2000 testing system between 1.0 V and 3.0 V at the scan rate of 0.1

mV/s. Electrochemical impedance spectroscopy (EIS) measurements were carried out over a frequency range of 10mHz –100KHz at 5 mV as the applied sinusoidal perturbation.

3. RESULTS AND DISCUSSIONS

3.1 Particles structures and phase identifications

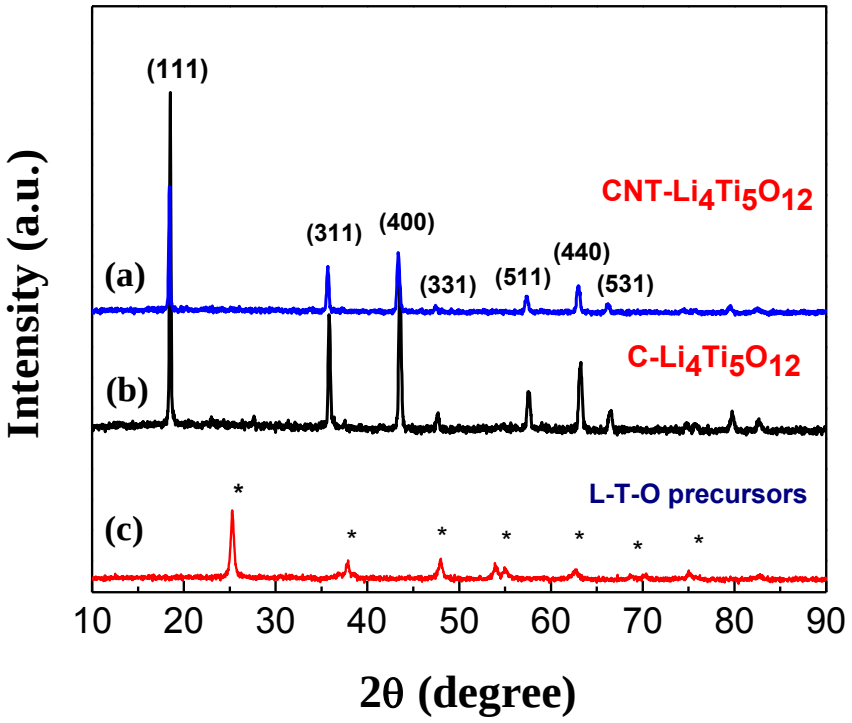

Figure 1. (a, b) XRD patterns of C-LTO and CNT-LTO nanocomposite particles and (**c**) the L-T-O precursors

The comparison of XRD patterns of two LTO samples and LTO precursor are shown in Fig. 1. It is noteworthy that the diffraction peaks of two LTO samples in Fig. 1(a, b) are in good agreement with JCPDS card No. 49-0207, and can be indexed to the spinel structure with the space group *Fd*3*m*, demonstrating the cubic spinel-$Li_4Ti_5O_{12}$ structure was indeed obtained. No crystalline carbon phase can be identified from XRD patterns, indicating that the coated carbon is amorphous with low content. It has also been suggested that the addition of carbon and CNTs to the precursor does not influence the formation of spinel-$Li_4Ti_5O_{12}$ during the heat-treatment, except for a weak peak in the pattern of CNT-LTO due to the CNTs in the composite. No other impurity phases are found compared with the LTO precursor at Fig.1(c), implying high-purity of spinel-$Li_4Ti_5O_{12}$ structure in both LTO samples.

The peaks of (111) and (311) in the XRD pattern were used to calculate average particle sizes using the Debye Scherrer's formula ($D = 0.9\lambda/\beta\cos\theta$, where λ = 0.154 nm (Cu Kα) and β = full width

half maximum at the diffraction angle of θ), and the estimated average sizes were summarized in Table 1.

Table 1. Comparison of the lattice parameters, average size, and average carbon content

	Before calcinations	After calcinations		
Sample	Carbon content (mass%)	Carbon content (mass%)	Lattice parameters (nm)	Average size (nm)
C-LTO	10%	3.8	0.8350	26.8
CNT-LTO	20%	9.4	0.8367	35.5

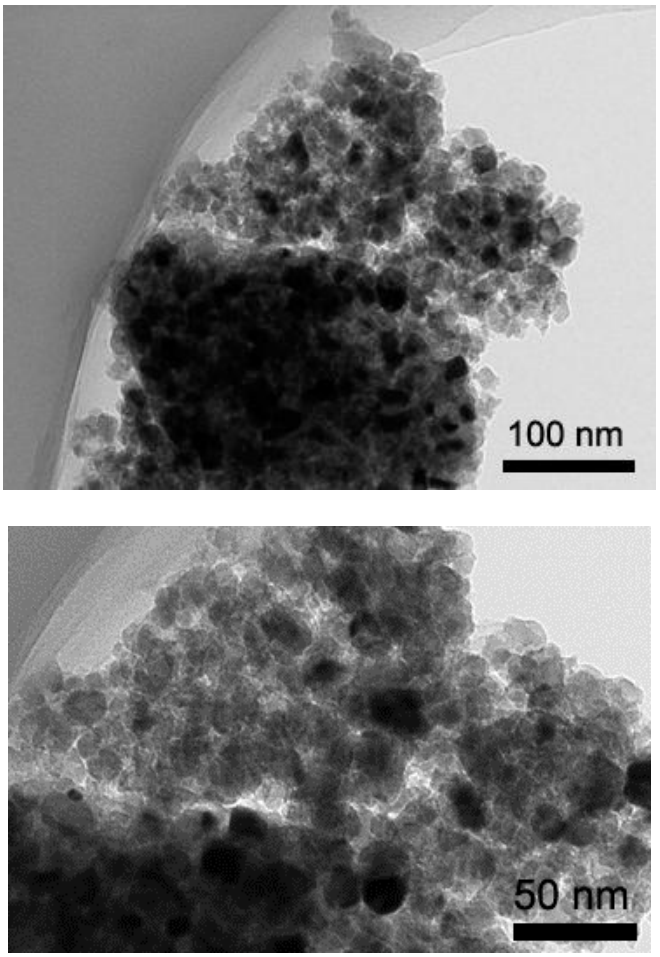

Figure 2. (a) Low magnification TEM micrographs of the C-LTO nanocomposite particles

Bragg equation was used to determine the lattice parameter, *a*, by $n\lambda = 2d_{nkl} \sin\theta$, where *n* is 1, λ is the wavelength of the incident X-ray beam (0.154 nm), *θ* is the incident angle, and *d* is the distance between the atomic layers of the cubic structure. Because $Li_4Ti_5O_{12}$ is face centered cubic, the lattice parameter can be calculated by using $d_{hkl} = a/D$, with $D=(h^2+k^2+l^2)^{1/2}$, and *a* as the lattice parameter and (h k l) as the Miller indices. The lattice parameters of two samples are also listed in

Table 1. It can be seen that the lattice parameters did not change significantly. In addition, average carbon content (mass fraction) of two LTO particles were measured from the quantitative energy-dispersive X-ray micro-analysis (SEM/EDX) and listed in Table 1. It is apparent that the average carbon content is less for C-LTO particles.

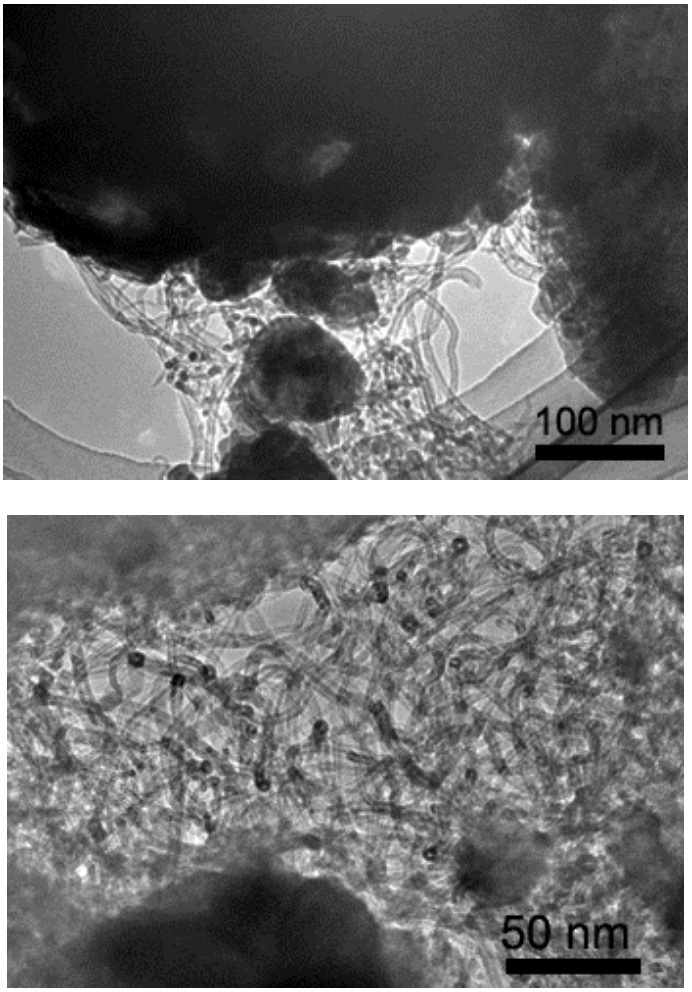

Figure 2. (b) Low magnification TEM micrographs of the CNT-LTO nanocomposite particles

Fig. 2a and 2b show the low magnification TEM micrographs of the C-LTO nanocomposite particles and CNT-LTO nanocomposite particles, respectively. It is obvious that both LTO particles are well dispersed with relatively uniform sphere-like nanostructures with sizes ranging of 20–70 nm. More importantly, it can be clearly seen in Fig. 2(b) that the CNT networks are dispersed among the CNT-LTO particles.

To further examine the nano-architectures, both LTO samples were investigated by HR-TEM. Fig. 3 and 4(a, b) show the HR-TEM images of an individual C-LTO and CNT-LTO particle, respectively. It is clear that both LTO particles exhibit a cubic nanocrystal with sizes between 20-70 nm. The C-LTO particles show the spherical shape with over 10 nm amorphous carbon uniformly coated on the surface. On the other hand, the CNT-LTO particles show uniform square morphologies

with edge length around 20 nm and a few layers of graphitic coating on the surface. The average sizes of both LTO particles agree well with the above XRD calculations. Furthermore, both HRTEM images reveal that the lattice fringes have an inter-planar spacing of 0.48 nm, consistent with the (111) atomic planes of the spinel structure, indicating a well-crystallized spinel phase.

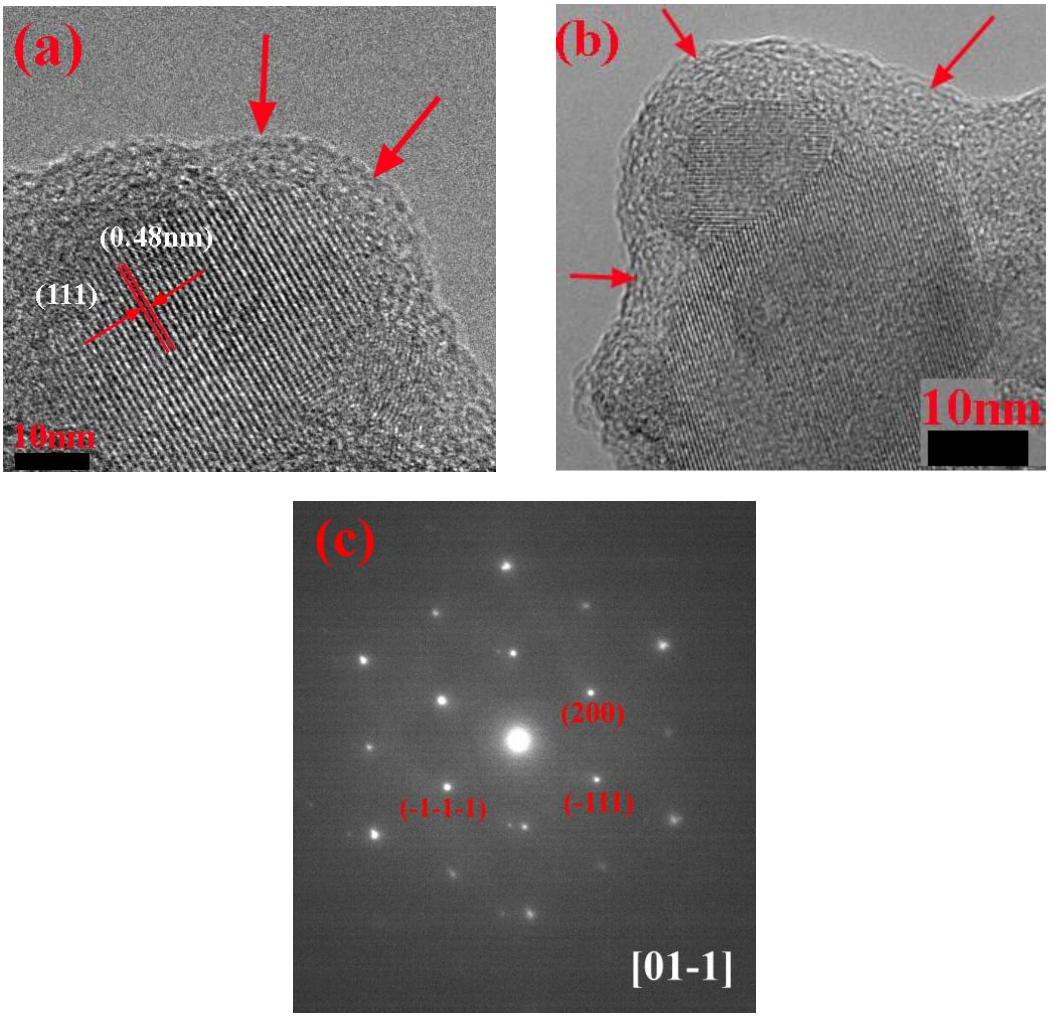

Figure 3. (a, b) HRTEM image of C-LTO particles and (**c**) SAED patterns of LTO nanocrystal

Fig. 3c and 4 c show the SAED patterns of both LTO nanocrystals. The SAED patterns can be indexed to be a single spinel phase, which again confirmed that the well-crystallized spinel cubic phase of $Li_4Ti_5O_{12}$ was formed during the calcination process for both types of LTO particles.

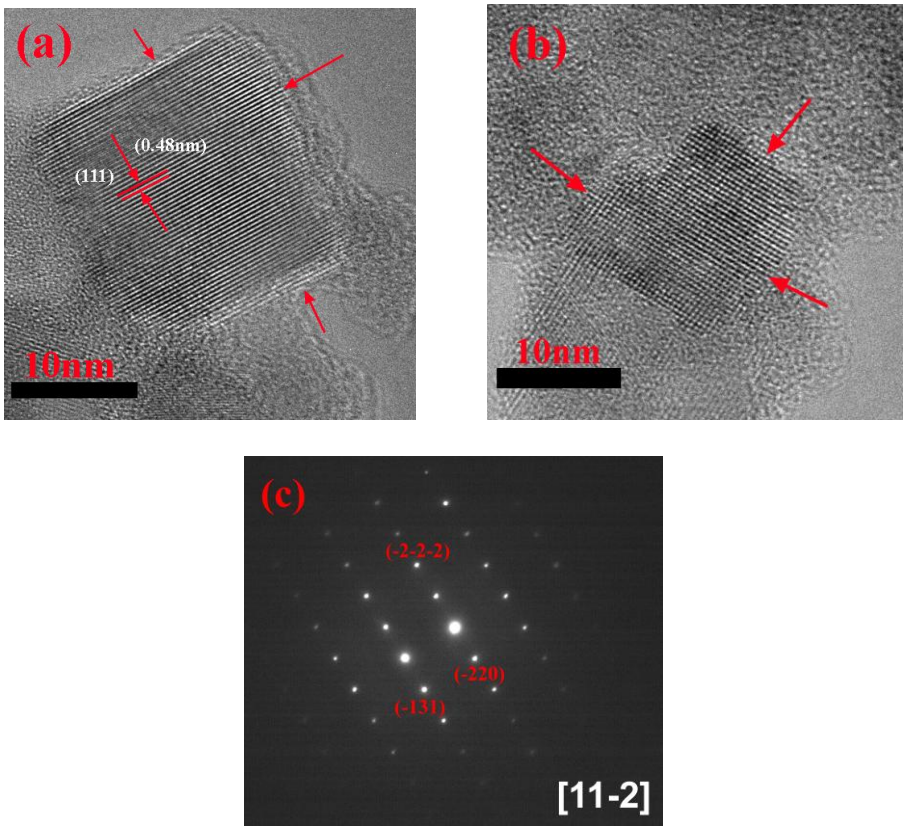

Figure 4. (a, b) HRTEM images of CNT-LTO particles and (**c**) SAED patterns of LTO nanocrystal

3.2 Electrochemical analysis

The electrochemical lithium insertion/extraction performance of the C-LTO and CNT-LTO nanocomposite electrodes was characterized by cyclic voltammograms (CV) within a potential window of 1.0–3.0 V (vs. Li/Li^+), and the CV profiles are shown in Fig.5. The CV curve of the C-LTO electrode is similar to that of the CNT-LTO electrode, with a pair of reversible redox peaks clearly observed. However, the anodic and cathodic peaks are sharper for the CNT-LTO composite, indicating a faster electrode kinetic process.

At a scan rate of 0.1 mV s^{-1}, the redox peak is located at 1.5 V/1.64 V (vs. Li/Li^+) for the C-LTO composite, while 1.47 V/1.55 V for the CNT-LTO composite. The potential difference between the oxidation and reduction peaks reflects the polarization degree of the electrode. The CNT-LTO electrode has a smaller potential difference than the C-LTO electrode, indicating a weaker polarization. This could be attributed to the following: 1) the smaller size means shorter distance for Li^+ ion diffusion inside LTO particles and thus faster diffusion process; 2) higher surface area of CNT-LTO nanocomposite provides a higher electrode/electrolyte contact area, which results in a low electrochemical reaction resistance during the rapid charge/discharge process.

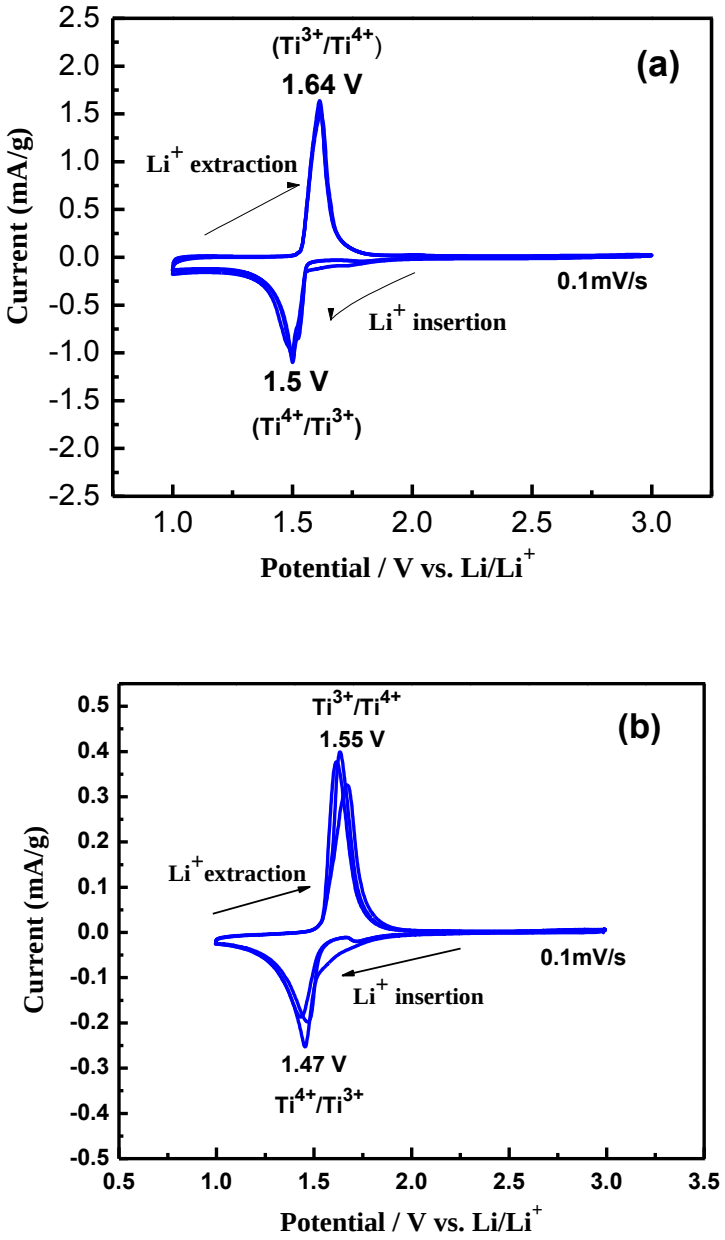

Figure 5. (a) Cyclic voltammograms of the C-LTO nanocomposites at scanning rate of 0.1mV/s, and **(b)** Cyclic voltammograms of the CNT-LTO nanocomposites at scanning rate of 0.1mV/s

Fig.6 shows the comparison of the charge-discharge capacity profiles of C-LTO and CNT-LTO particles at different C rates (from 0.1*C* to 2*C*) in a voltage range between 3.0 V and 1.0 V. Both particles showed the superior initial discharge capacity of 200 mAh/g at 1/10C, which is more than the theoretical capacity of 175 mAh/g, indicating the existence of additional lithium storage sites at first cycle of the reduction/oxidation reaction for C-LTO and CNT-LTO nanoparticles.

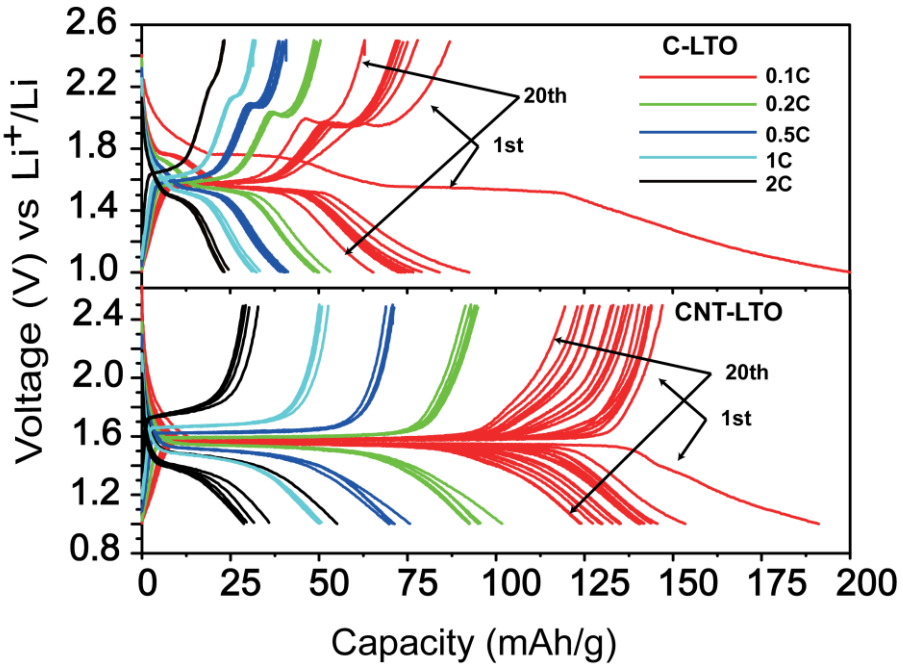

Figure 6. The charge-discharge capacity profiles for Li^+ ions insertion-extraction of C-LTO and CNT-LTO nanocomposite particles at various *C* rates

The charge-discharge cycling behavior is a typical kinetic reaction of $Li_4Ti_5O_{12}$ with a flat charge–discharge plateau at an average potential of 1.55 V (vs. Li/Li^+), which is attributed to a two-phase phenomenon pertaining to $Li_4Ti_5O_{12}$ phase and $Li_7Ti_5O_{12}$ phase. This intercalation and de-intercalation process can be expressed as $Li_4Ti_5O_{12}+3Li^++3e \rightleftharpoons Li_7Ti_5O_{12}$ [1-14].

It is also clearly seen from Fig. 6 that the first discharge and charge capacities at 1/10 C of CNT-LTO were as high as ~200 and ~155 mAh/g, respectively, corresponding to a Coulombic efficiency of 77.5%. The first discharge and charge capacities of C-LTO were ~200 and ~90 mAh/g with Coulombic efficiency of 45%. Both initial irreversible capacity losses (i.e. the difference on first discharge-charge capacity) would possibly be resulted from irreversible lithium loss due to the formation of solid electrolyte interphase (SEI) film along with carbon modification [30, 31]. The comparison of Coulombic efficiency suggested that the amorphous carbon coating of C-LTO particles is much thicker than the few graphitic layers on the CNT-LTO particles. A thick carbon coating resulted in the decrease in the discharge capacity and increase in polarization at more cycling [32]. On the contrary, uniform and thin coating layers on the $Li_4Ti_5O_{12}$ offer a large effective reaction area favorable for charge-transfer and Li^+ ion diffusion. After first discharge and charge cycle at 0.1C, further lithium ions insertion/extraction into/from the $Li_4Ti_5O_{12}$ electrode exhibited a very good reversible behavior for the CNT-LTO nanoparticles. Apparently, the CNT-LTO particles have a larger reversible capacity (e.g., 120-160 mA·h/g) than the reversible capacity (e.g., 75-120 mA·h/g) of the C-LTO particles. In addition, the CNT-LTO particles show very good reversible symmetry of charge–discharge from 0.1C to 2C. On the contrary, the C-LTO particles exhibit an asymmetry of charge–discharge cycling, and sharp step increases of the voltage occurred during the charging process due to an irreversible electrode polarization. Indeed, it is believed that the difference in the charge–discharge

profile may be ascribed to the agglomeration of C-LTO nanoparticle and excessive amorphous carbon among LTO particles [27, 33, 34]. Such an irreversible capacity of the LTO particles is probably correlated with its final $Li_4Ti_5O_{12}$ crystal structure. Usually some minor amounts of residual anatase TiO_2, even if it was difficult to detect from XRD in Fig. 1 (b, c), resulted in low electrochemical reactivity. Other possible reasons could be the surface defects such as surface voids and the dissolution of surface impurities [32, 35, 36] such as adsorbed traces of water from the electrodes into the liquid electrolyte. This is detrimental for the Li^+ exchange and decreases the capacity and gives rise to higher irreversibility.

As is known, nanoscale electrode materials (i.e. cathode and anode) have demonstrated an enhanced performance for in Li-ion batteries by providing higher electrode/electrolyte contact area, shorter Li^+ diffusion length (L) and faster electron transport in the intercalation host (smaller time constant $\tau = L^2/2D$, where D is the coupled diffusion coefficient for both Li^+ and e), and better accommodation of the Li-ion insertion/extraction [28, 29]. Our current CNT-LTO particles have a larger reversible charge-discharge capacity of 120-160 mA·h/g at 0.1C and 0.2C. We propose that the interconnected CNT networks among the isolated $Li_4Ti_5O_{12}$ particles provided conductive networks [37, 22], resulting in excellent Li^+ insertion/extraction performance, easier and shorter diffusion pathways for ionic and electronic diffusion, and thus higher discharge capacity. Moreover, the addition of carbon nanotubes to the precursor hinders particle agglomeration and growth during the high-temperature calcination process, resulting in uniform particle size and square morphology, which reduces the distance for lithium ion diffusion and increases the electrode/electrolyte contact surface area. The graphitic layer coated on the surface of $Li_4Ti_5O_{12}$ particles is also favorable for improving the electronic conductivity.

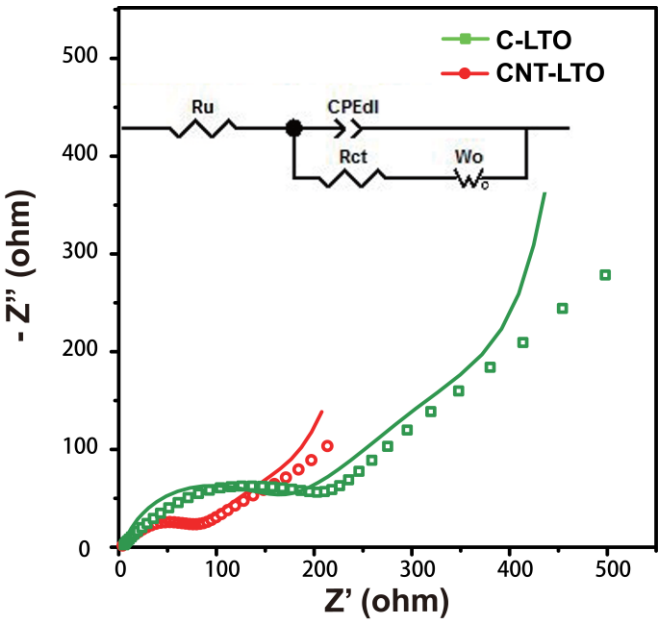

Figure 7. The EIS Nyquist plots of C-LTO and CNT-LTO nanocomposite electrodes. Frequency range is from10 mHz to100 KHz. The inset figure show the corresponding equivalent circuit Randle model

In order to further clarify and compare the two nanocomposite electrode performance as related to the electrode kinetics, electrochemical impedance spectroscopy (EIS) was carried out over the frequency range of 10mHz – 100KHz for both C-LTO and CNT-LTO electrodes in the fully charged state. The Nyquist plots and the fitting results using an equivalent circuit are given in Fig.7. Both Nyquist plots are composed of a depressed semicircle in high frequency and a straight line in low frequency region. The solution resistance *Ru* of the cell deducted from $Z^{'}$ axis interception at high frequency includes both electrolyte and electrode contact resistance. The charge transfer resistance *Rct* is determined by the semicircle in the middle frequency range, which is mainly related to the electrochemical reaction at the electrolyte/electrode interface. The straight line in low frequency range is attributed to the Warburg impedance *Wo*, which is due to the solid-state diffusion of Li^+ ions into the bulk of active material. It can be seen from Fig.7 that the CNT-LTO electrode displayed much lower impedance than that of C-LTO, which is similarly observed in the literature [38, 39]. The equivalent circuit model is depicted in the inset of Fig. 7, where *Ru* and *Rct* are solution resistance and charge transfer resistance, respectively, and CPE is the Constant Phase Element involving double layer capacitance of the electrolyte-electrode interface.

The equivalent circuit model is fitted well to the experimental data and the fitting results of the EIS data for the C-LTO and CNT-LTO electrodes are given in Table 2. It can be seen that the *Ru* and *Rct* are much smaller for the CNT-LTO electrode (*Ru* = 3.43Ω, *R*ct = 59.95Ω) than for the C-LTO (*Ru* = 4.24Ω, *Rct* = 150.8Ω).

Table 2. Comparison of the Ru and Rct values

Sample	Ru (Ω)	Rct (Ω)
C-LTO	4.24	150.8
CNT-LTO	3.43	59.95

This result indicates that the CNT coating has enabled easier charge transfer at electrode/electrolyte interface, and a decrease in the overall battery internal resistance. The results are consistent with the charge/discharge curves shown in Fig.6 and lithium insertion/extraction shown in Fig.5. Overall, the conductive graphitic layers and CNT interconnection networks facilitate electronic conductive paths in the LTO particle surroundings, which are considered a key factor in improving the discharge capacity and rate of Li^+ insertion/extraction in the CNT-LTO materials.

According to the recent report [40], the appropriate amount of residual anatase TiO_2 in final LTO phase particles could be beneficial to improving its electrochemical performances. It is also reported that there is a strong synergistic effect between $Li_4Ti_5O_{12}$ and TiO_2 in $Li_4Ti_5O_{12}$-TiO_2 nanocomposite system with hierarchical structures, as anatase TiO_2 could partly contribute to the total reversible capacity [41, 42]. On the other hand, the mixed secondary TiO_2 impurity phase will also lead to more polarization and more irreversible capacity loss at higher rates. This indicates that the optimization of anatase TiO_2 as one of precursors during the preparations is critical for improving the electrochemical performance.

4. CONCLUSIONS

Spinel-type C-LTO and CNT-LTO nanocomposite particles have been synthesized. Comparative nanostructure analyses (XRD, HRTEM and SAED) and electrochemical testing (charge-discharge, CV and EIS) revealed that the C-LTO particles have excessive carbon coating on the surface, resulting in a high irreversible capacity. The CNT-LTO particles have thinner graphitic layers covering the nanocrystal surface and higher reversible charge–discharge capacity than that of the C-LTO particles at different rates, which is ascribed to the synergistic effect of thinner graphitic layers and CNT interconnection networks of the electrode materials that provide shorter diffusion-paths and faster migration rate of both ions and electrons. This work demonstrates that the CNT-LTO nanocomposite particles have the improved capacitive performance, making it an efficient and highly promising material for use in the development of rechargeable Li-ion cells. The current facile reaction technique represents an effective method for synthesizing $Li_4Ti_5O_{12}$ anode material for lithium ion batteries.

ACKNOWLEDGEMENTS

The President's Award of University of Waterloo and Postgraduate Scholarships from the Natural Sciences and Engineering Research Council of Canada (NSERC) and Nano-fellowship from Waterloo Institute for Nanotechnology (WIN) are greatly appreciated by XC Sun. Financial supports of Beijing Nova Program (2010B008) and Beijing Natural Science Foundation (2132014) are greatly appreciated by YF Zhang. Thanks to Dr. Kai Sun at University of Michigan and Dr. Xuedong Bai at Institute of Physics in Chinese Academy of Sciences for their valuable discussions on HRTEM images processing. Thanks for Mr. Shanming Li on his helps in TEM imaging at Beijing National Laboratory for Condensed Matter Physics, Institute of Physics, Chinese Academy of Sciences, China. Special thanks for Prof. Juewen Liu's groups on the helps in samples preparation at Chemistry Department, University of Waterloo.

References

1. K. Zaghib, M. Simoneau, M. Armand, *J. Power Sources*, 81(1999) 300
2. K. Zaghib, M. Armand, M. Gauthier, *J. Electrochem. Soc*., 145 (1998) 3135
3. T. Ohzuku, A. Ueda, N. Yamamoto, *J. Electrochem. Soc*., 142 (1995) 1431
4. E. Ferg, R.J.Gummow, A. de Kock, M. M. Thackeray, *J. Electrochem. Soc*., 141 (1994) L147
5. S. W. Woo, K. Dokko, K. Kanamura, *Electrochim. Acta*, 53 (2007) 79
6. L. Cheng, H. J. Liu, J. J. Zhang, H. M. Xiong Y. Y. Xia, *J. Electrochem. Soc*., 153 (2006) A1472
7. J. R. Li, Z. L. Tang, Z. T. Zhang, *Electrochem. Commun*., 7 (2005) 894
8. C. H. Jiang, M. Ichihara, I. Honma, H. S. Zhou, *Electrochim. Acta* , 52 (2007) 6470
9. S. Huang, M. Woodson, R. Smalley, J. Liu, *Nano Lett*., 4 (2004) 1025
10. H. G. Jung, M. W. Jiang, J. Hassoun, Y. K. Sun, B. Scrosati, *Nat. Commun*., 2 (2011) 516
11. Z. Liang, Y. S. Hu, H. Li, Z. X. Wang, L. Q. Chen, *Adv. Mater*., 23 (2011) 1385
12. G. D. Gu, N. Sharma, V. K. Peterson, J. A. Kimpton, D. Z. Jia, Z. P. Guo, *Adv. Funct. Mater*., 21 (2011) 3990
13. T. F. Yi, J. Shu, X. D. Zhu, Y. R. Zhu, C. B. Yue, A. N. Zhou, R. S. Zhu, *Electrochim. Acta*, 54 (2009) 7464

14. K. Amine, I. Belharouak, Z. H. Chen, T. Tran, H. Yumoto, N. Ota, S.T. Myung, Y. K. Sun *Adv. Mater*., 22 (2010) 3052
15. Y. Wang, H. Liu, K. Wang, H. Eiji, Y. Wang, H. Zhou, *J. Mater. Chem*., 19 (2009) 6789
16. Z. J. Ding, L. Zhao, L.M. Suo, Y. Jiao, S. Meng, Y.S. Hu, Z. X. Wang, L.Q. Chen, *Phys. Chem. Chem. Phys.*, 13 (2011) 15127
17. H. W. Lu, W. Zeng, Y. S. Li, Z. W. Fu, *J. Power Sources*, 164 (2007) 874
18. J. Y. Kim, J. P. Cho, *Electrochem. Solid-State Lett*., 10 (2007) A81
19. A. S. Prakash, P. Manikandan, K. Ramesha, M. Sathiya, J. M. Tarascon, A. K. Shukla, *Chem. Mater*., 22 (2010) 2857
20. E. M. Sorensen, S. J. Barry, H. K. Jung, J. R. Rondinelli, J. T. Vaughey, K. R. Poeppelmeier, *Chem. Mater*., 18 (2006) 482
21. G. Zhu, H. Liu, J. Zhuang, C. Wang, Y.Y. Xia, *Energy Environ. Sci*., 4 (2011) 4016
22. L. Cheng, J. Yan, G. N. Zhu, J. Y. Luo, Y. Y. Xia, *J. Mater. Chem*., 20 (2010) 595
23. J. Gao, J. R. Ying, C. Y. Jiang, C. R. Wan, *J. Power Sources*, 166 (2007) 255
24. J. J. Huang, Z. Y. Jiang, *Electrochim. Acta*, 53 (2008) 7756
25. K. S. Park, A. Benayad, D.J. Kang, S. G. Doo, *J. Am. Chem. Soc*., 130 (2008) 14930
26. H. K. Kim, S. M. Bak, K. B. Kim, *Electrochem. Communication*, 12 (2010) 1768
27. B. H. Li, F. Ning, Y. B. He, H. D. Du, Q.H. Yang, J. Ma, F.Y. Kang, C.T. Hsu, *Int. J. Electrochem. Sci*., 6, (2011) 3210
28. K. Amine, I. Belharouak, Z. H. Chen, T. Tran, H. Yumoto, N. Ota, S. T. Myung, Y. K. Sun, *Adv. Mater*., 22 (2010) 3052
29. Y. Ren, A. R. Armstrong, F. Jiao, P. G. Bruce, *J. Am. Chem. Soc*., 132(2010) 996
30. Z. S. Wu, W. Ren, L. Wen, L. Gao, H. M. Cheng, *ACS Nano*, 4 (2010) 3187
31. Y. Shi, L. Wen, F. Li, H. M. Cheng, *J. Power Sources*, 196 (2011) 8610
32. L. Shen, C. Yuan, H. J. Luo, X. Zhang, H. Xu, Y. Xia, *J . Mater. Chem*., 20 (2010) 6998.
33. J. H. Ryu, *J. Electrochemical Sci. Tech*., 2 (2011) 136
34. W. J. H. Borghols, M. Wagemaker, U. Lafont, E. M. Kelder, F. M. Mulder, *J. Am. Chem. Soc.*, 131 (2009) 17786
35. J. Liu, X. F. Li, J. Yang, D. S. Geng, Y. L. Li, D. Wang, R. Li, X. L. Sun, M. Cai, M. W. Verbrugge, *Electrochim. Acta*, 63 (2012) 100
36. J. Chen, L. Yang, S. Fang, Y. Tang, *Electrochim. Acta*, 55 (2010) 6596
37. X. Li, M. Z. Qu, Y. J. Huai, Z .L. Yua, *Electrochim. Acta*, 55 (2010) 2978
38. T. Yuan, X. Yu, R. Cai, Y. Zhou, Z. Shao, *J. Powder Sources*, 195 (2010) 4997
39. L. Yang, J. Gao, *J. Alloys & Compounds*, 485 (2009) 427
40. L. L. Xie, Y. D. Xu, J. J. Zhang, X. Y. Cao, B. Wang, X. Y. Yan, L. B. Qu, *Int. J. Electrochem. Sci*., 8 (2013) 1701
41. Y. Q. Wang, L. Gu, Y. G. Guo, H. Li, X. Q. He, S. Tsukimoto, Y. Ikuhara, L. J. Wan, *J. Am. Chem. Soc*., 134 (2012) 7874
42. J. Wang, H. Zhao, Q. Yang, C. M. Wang, Q. Xia, *J. Powder Sources*, 222 (2013) 196